This is an open access article published under an ACS AuthorChoice License, which permits copying and redistribution of the article or any adaptations for non-commercial purposes.

ACS OMEGA

Article

Cite This: ACS Omega 2017, 2, 7389-7399

http://pubs.acs.org/journal/acsodf

Site-Specific Fluorescence Dynamics To Probe Polar Arrest by Fob1 in Replication Fork Barrier Sequences

Anwesha Biswas,[†,§] Jessy Mariam,[†,§] Mamta Kombrabail,[‡] Satya Narayan,[‡] G. Krishnamoorthy,*[,†,‡,∥] and Ruchi Anand*[,†]

[†]Department of Chemistry, Indian Institute of Technology Bombay, Mumbai, Maharashtra 400076, India

[‡]Department of Chemical Sciences, Tata Institute of Fundamental Research, Mumbai, Maharashtra 400005, India

Supporting Information

ABSTRACT: Fob1 protein plays an important role in aging and maintains genomic stability by avoiding clashes between the replication and transcription machinery. It facilitates polar arrest by binding to replication fork barrier (RFB) sites, present within the nontranscribed spacer region of the ribosomal DNA. Here, we investigate the mechanism of unidirectional arrest by creating multiple prosthetic forks within the RFB, with fluorescent adenine analogue 2-aminopurine incorporated site-specifically in both the "permissible" and "nonpermissible" directions. The motional dynamics of the RFB-Fob1 complexes analyzed by fluorescence lifetime and fluorescence anisotropy decay kinetics shows that Fob1 adopts a clamp-lock model of arrest and causes stronger perturbation with the bases in the double-stranded region of the nonpermissible-directed forks over those of the permissible directed ones, thereby creating a polar barrier. Corroborative thermal melting studies reveal a skewed distribution of GC content within the RFB sequence that potentially assists in Fob1-mediated arrest.

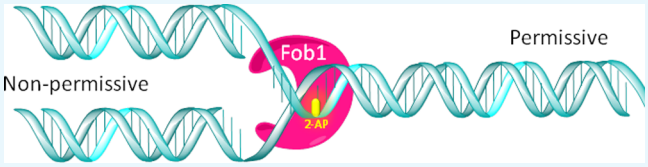

INTRODUCTION

Pause of DNA replication forks at certain physiologically programmed sites within the genome has been observed in prokaryotes and eukaryotes alike.[1] These sites have been programmed for a variety of functions, from the maintenance of fidelity in the replication process to the avoidance of clashes between the replication and transcription machinery.[2,3] In prokaryotes, this occurs during the bidirectional replication of the circular genome, and the process has been thoroughly investigated both structurally and mechanistically.[4,5] Analogous replication fork barrier (RFB) sites have been observed in eukaryotes in the ribosomal DNA (rDNA) repeat regions (100−200 repeats)[6−9] (Figure S1), where polar arrest proteins like Fob1 (fork blocking) in yeast enforce unidirectional transcription and replication. During replication, these repeats get stochastically excised by recombination[10] at the stalled forks and is one of the causes of aging in yeast.[11]

Intriguingly, the eukaryotic RFB systems do not exhibit any similarity both at the DNA and the protein level with the prokaryotic system. Moreover, since the discovery of Fob1, there has been very little information regarding its domain organization and the mode of binding of Fob1 to RFB sites. Earlier bioinformatics studies had proposed that it has a zinc finger motif that partakes in DNA binding.[12,13] Till date, because of the paucity of the X-ray structure, limited knowledge regarding its molecular mechanism of arrest is available. The polar nature of Fob1-mediated arrest was first demonstrated by Brewer et al. who, by employing two-dimensional gel electrophoresis, were able to show blocking of replication intermediates.[14] It was demonstrated that accumulation of forks occurred only in an orientation-dependent manner and forks that approach from the direction of 5S rRNA transcription are arrested. However, the oppositely directed fork can pass through the site, unimpeded.[14,15] Moreover, this fork-blocking property was shown to be independent of transcription as it occurred even in RNA polymerase 1 knockout strains, thereby reasserting that RFB activity is sequence-specific. To understand the mechanism by which fork blocking occurs in this eukaryotic system, we have undertaken a thorough in-depth study of the DNA recognition element responsible for fork stalling. A series of prosthetic forked DNA constructs were designed, with the fork progressing to different extents as well as progressing from different directions within the *RFB* (*ter*) sequence (Figures S2 and S3). The directions of the approaching fork have been termed "permissible" or "non-permissible" depending on whether they are approaching from the reported passive direction and are allowed to pass through the RFB site or arrested, respectively. Fluorescent adenine analogue 2-aminopurine (2-AP) has been used as a reporter of the local environment,[16−20] and this probe has been incorporated site-specifically in the prosthetic forks that were constructed. A combination of thermal melting studies, fluorescence lifetime, and fluorescence anisotropy decay kinetics was performed in the presence and absence of Fob1 to aid in deciphering the mechanism of DNA recognition and polar arrest by this protein. The results show that the Fob1

Received: August 2, 2017
Accepted: October 12, 2017
Published: October 30, 2017

© 2017 American Chemical Society

DOI: 10.1021/acsomega.7b01117
ACS Omega 2017, 2, 7389−7399

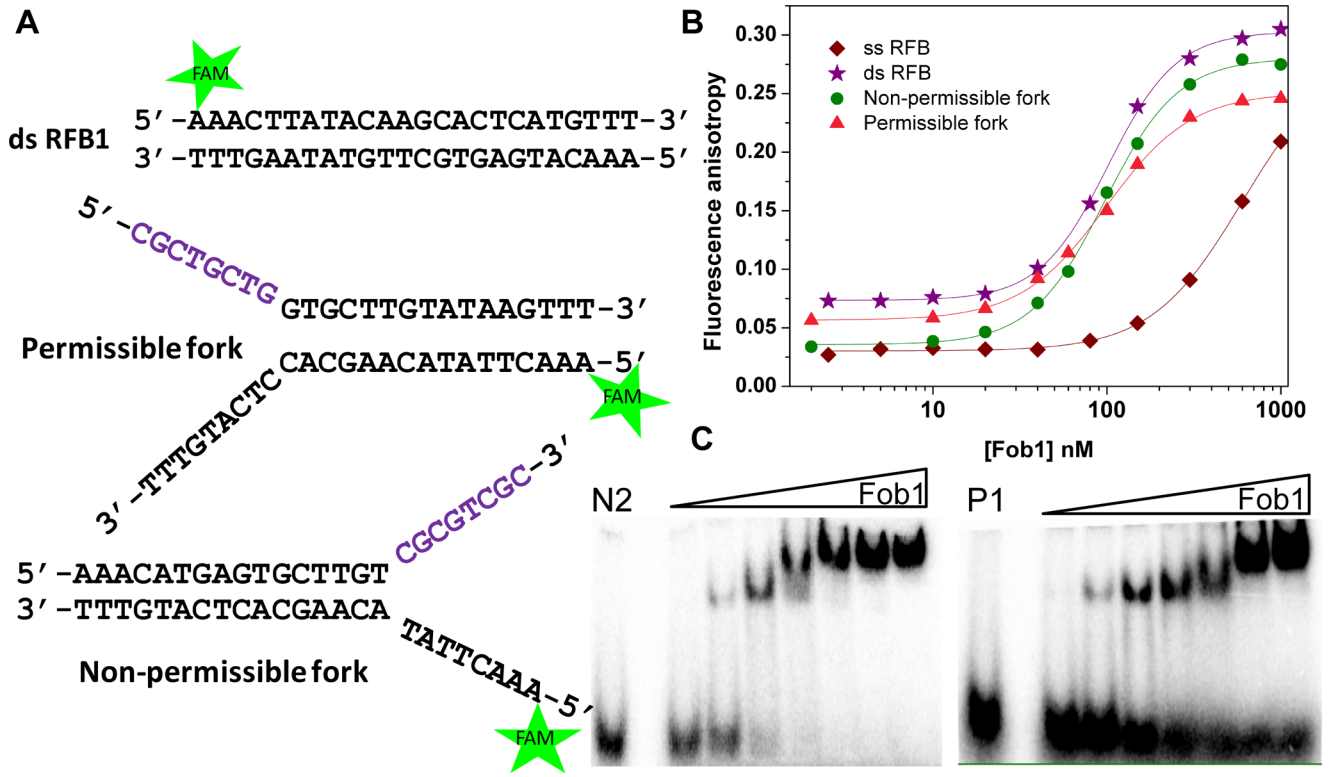

Figure 1. Steady-state fluorescence anisotropy and EMSA studies of *ter* with Fob1. (A) Schematic representation of 5′-6-FAM-labeled constructs. The sequence in purple represents the non-natural mismatched bases introduced to create the fork. (B) Steady-state anisotropy titration curves of single-stranded, double-stranded, nonpermissible, and permissible RFB1 forks with Fob1. (C) Electrophoretic mobility gel shift assay of nonpermissible (N2) and permissible (P1) forks in the presence of 0.06, 0.13, 0.26, 0.52, 1.05, 2.1, and 4.2 μM Fob1.

protein causes polar arrest by preferentially interacting with the double-stranded region, a few bases ahead of the nonpermissive directed fork by acting as a unidirectional clamp.

RESULTS AND DISCUSSION

Fob1 from *Ashbya gossypii*, a close homologue of *Saccharomyces cerevisiae*, was used as a model system to establish the mechanism of polar arrest. The *Ashbya gossypii* Fob1 protein was identified from a BLAST search as a close homologue, and we believe both fungi adopt a common mechanism of regulation. The intergenic NTS1 region, which contains the *ter* sequences, is highly conserved across fungal species. In fact, in the case of *S. cerevisiae* and *A. gossypii*, the *ter*1 sequence is identical. Therefore, the choice of protein should not affect the interpretations. This Fob1 construct was used due to ease of purification, solubility, and stability of the protein. Because this particular protein has not been characterized earlier, to confirm its ability to bind the *ter*1 sequence and to gain an estimate of its binding constant under steady-state conditions, bulk fluorescence anisotropy experiments were carried out with the 5′-6-FAM-labeled *ter* sequence (Figure 1A). Results reveal that Fob1 is able to bind both the double-stranded and forked sequences with similar affinity (Figure 1B) and exhibits 10-fold less affinity for single-stranded *ter*. The confirmatory electrophoretic mobility gel shift assay (EMSA) with various fork constructs in both permissible and nonpermissible directions (Figure 1C) was instrumental in reaffirming our findings. Armed with this information, site-specific experiments were undertaken.

Artificial forks where an adenine analogue, 2-AP, was substituted only at the natural adenine sites in the double-stranded region are labeled with a postscript "D*", and when it was substituted at the fork, it was labeled as "F*". A prescript of "N" or "P" has been added for nonpermissible/permissible directed forks, and for sequences where 2-AP was incorporated at the fork junction, a postscript of "tD" has been used. Fluorescence anisotropy decay kinetics data was fit satisfactorily to a sum of two exponentials, where the local dynamics of the base in the DNA strand was represented by the faster rotational correlation time (ϕ_1), whereas the global motion of the entire DNA or the complex was represented by the slower rotational correlation (ϕ_2). Order parameter S^2 (eq 6) for the probe was subsequently calculated.[21]

Anomalous Behavior of 2-AP at Forks. Free 2-AP has a single fluorescence lifetime of 11 ns but when incorporated within a DNA, 2-AP exhibits upto four lifetimes with the shortest lifetime (τ_1, 20−70 ps; Table 2) ascribed to base-pairing and the associated stacking interactions between bases.[22] The longest lifetime is attributed (5−9 ns, Table 2) to an extrahelical component, and the origin of the middle two lifetime components (0.2−0.6 and 1.5−3 ns) is presumed to represent conformations in between the completely stacked state and extrahelical state. Because of the inability to assign the middle two lifetime components, we prefer to use the mean lifetime (τ_m) in differentiating the mode of binding of Fob1 (see below). However, the observed variation in the mean lifetime reflects the relative contributions of the shortest and the longest lifetime components. Increase in the mean lifetime caused by Fob1 binding (see later) arises mainly due to increase in the value of the shortest lifetime component and a concomitant decrease in its amplitude, which reflect weakening of base-pairing. Thus, the change in the value of mean lifetime

DOI: 10.1021/acsomega.7b01117
ACS Omega 2017, 2, 7389−7399

Table 1. Fluorescence Lifetime and Anisotropy Parameters of 2-AP in DNA and DNA−Protein Complexes[a]

Sequence		Mean lifetime τ_m (ns)			S^2		
		ss	ds	ds_Fob1	ds	ds_Fob1	ΔS^2
N1F*	TCTAAACTTA*TACAAGCACTCATGTTTGCC	0.48 ± 0.03	0.64 ± 0.04	1.12 ± 0.12	0.40 ± 0.01	0.54 ± 0.04	0.14 ± 0.04
N1D*	TCTAAACTTATACAA*GCACTCATGTTTGCC	0.50 ± 0.01	0.57 ± 0.02	1.57 ± 0.09	0.15 ± 0.04	0.58 ± 0.03	0.43 ± 0.05
N2F*	ACTTATACAA*GCACTCATGTTTGCCGCTCT	0.45 ± 0.07	1.10 ± 0.09	1.79 ± 0.07	0.37 ± 0.03	0.60 ± 0.02	0.23 ± 0.04
N2D*	ACTTATACAAGCACTCA*TGTTTGCCGCTCT	3.16 ± 0.14	0.090 ± 0.005	0.25 ± 0.01	0.27 ± 0.02	0.65 ± 0.01	0.38 ± 0.02
N3F*	TATACAAGCA*CTCATGTTTGCCGCTCTGAT	0.24 ± 0.04	1.00 ± 0.02	1.36 ± 0.17	0.31 ± 0.02	0.46 ± 0.02	0.15 ± 0.03
N3D*	TATACAAGCACTCA*TGTTTGCCGCTCTGAT	2.43 ± 0.08	0.25 ± 0.01	0.69 ± 0.07	0.18 ± 0.05	0.55 ± 0.01	0.37 ± 0.05
P4F*	TTCTCTAAACTTATACAAGCA*CTCATGTTT	0.50 ± 0.07	2.21 ± 0.04	2.85 ± 0.03	0.31 ± 0.01	0.52 ± 0.01	0.21 ± 0.01
P4D*	TTCTCTAAACTTATA*CAAGCACTCATGTTT	0.70 ± 0.05	0.16 ± 0.01	0.22 ± 0.01	0.36 ± 0.04	0.60 ± 0.04	0.24 ± 0.06
P1D*	TCTAAACTTATACAA*GCACTCATGTTTGCC	0.50 ± 0.01	0.69 ± 0.08	1.34 ± 0.15	0.19 ± 0.01	0.49 ± 0.02	0.30 ± 0.02
P5F*	CAATTCTCTAAACTTATACAA*GCACTCATG	0.38 ± 0.01	0.51 ± 0.02	0.80 ± 0.08	0.49 ± 0.01	0.63 ± 0.02	0.14 ± 0.02
NtD*	ACTTATACAA*GCACTCATGTTTGCCGCTCT	0.45 ± 0.07	2.28 ± 0.30	3.21 ± 0.26	0.31 ± 0.05	0.48 ± 0.02	0.17 ± 0.05
PtD*	CAATTCTCTAAACTTATACAA*GCACTCATG	0.38 ± 0.01	0.19 ± 0.02	0.28 ± 0.02	0.46 ± 0.02	0.51 ± 0.01	0.05 ± 0.02

[a]The table shows the 2-AP-incorporated modified DNA sequences with the bases of the *ter*1 sequence shown in bold and 2-AP represented as "A*" in red; the bases that are double-stranded after annealing have been underlined, and the rest of the sequence forms the forked region. After the sequence, the table includes the respective mean fluorescence lifetime (τ_m) of 2-AP in the single-stranded construct (ss), in the annealed construct (ds), and in the complex of the annealed construct with Fob1 (ds_Fob1); the next panel comprises the order parameter (S^2) of 2-AP in the annealed construct (ds) and in the complex (ds_Fob1) and the change in the order parameter caused by Fob1 binding (ΔS^2).

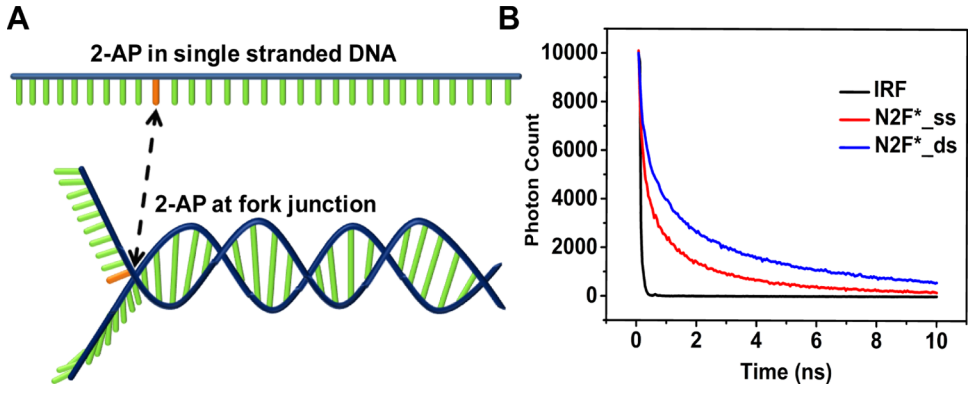

Figure 2. Anomalous behavior of 2-AP at forks: (A) Representations of the single-stranded construct and the construct with 2-AP (orange) at the fork position. (B) Fluorescence decay traces of 2-AP in N2F*_ss (red) and N2F*_ds (blue) and the IRF (black).

DOI: 10.1021/acsomega.7b01117
ACS Omega 2017, 2, 7389−7399

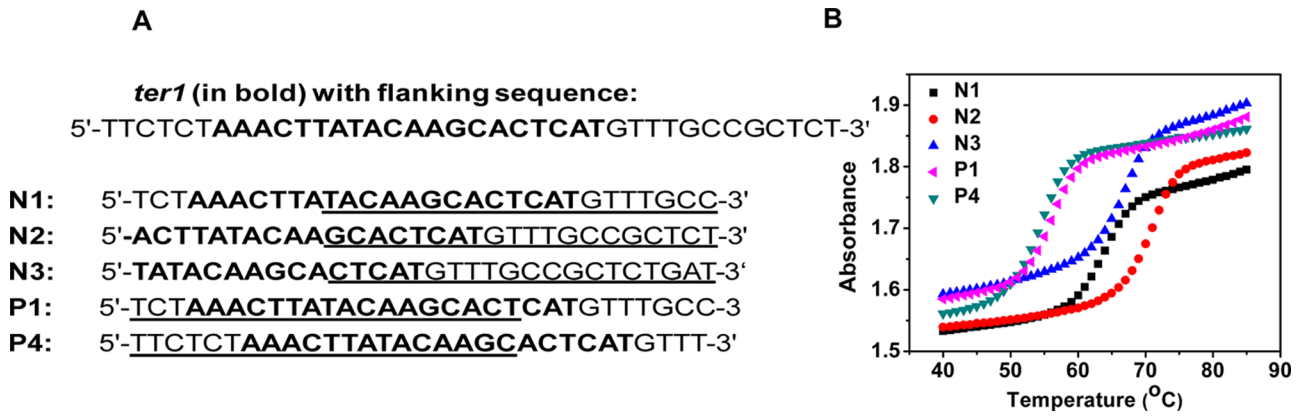

Figure 3. Effect of fork direction on *ter*1: (A) Prosthetic fork constructs were designed within the *ter*1 sequence along with its flanking sequences; bases in bold constitute the *ter*1 sequence; for the constructs, underlined bases represent the bases that are double-stranded after annealing, whereas the rest constitute the fork created by presenting the bases with mismatched sequences; mismatch at the 5′ end represents forks directed from the nonpermissible end, whereas the mismatch at the 3′ represents forks directed from the permissible end. (B) Thermal melting profile of the constructs.

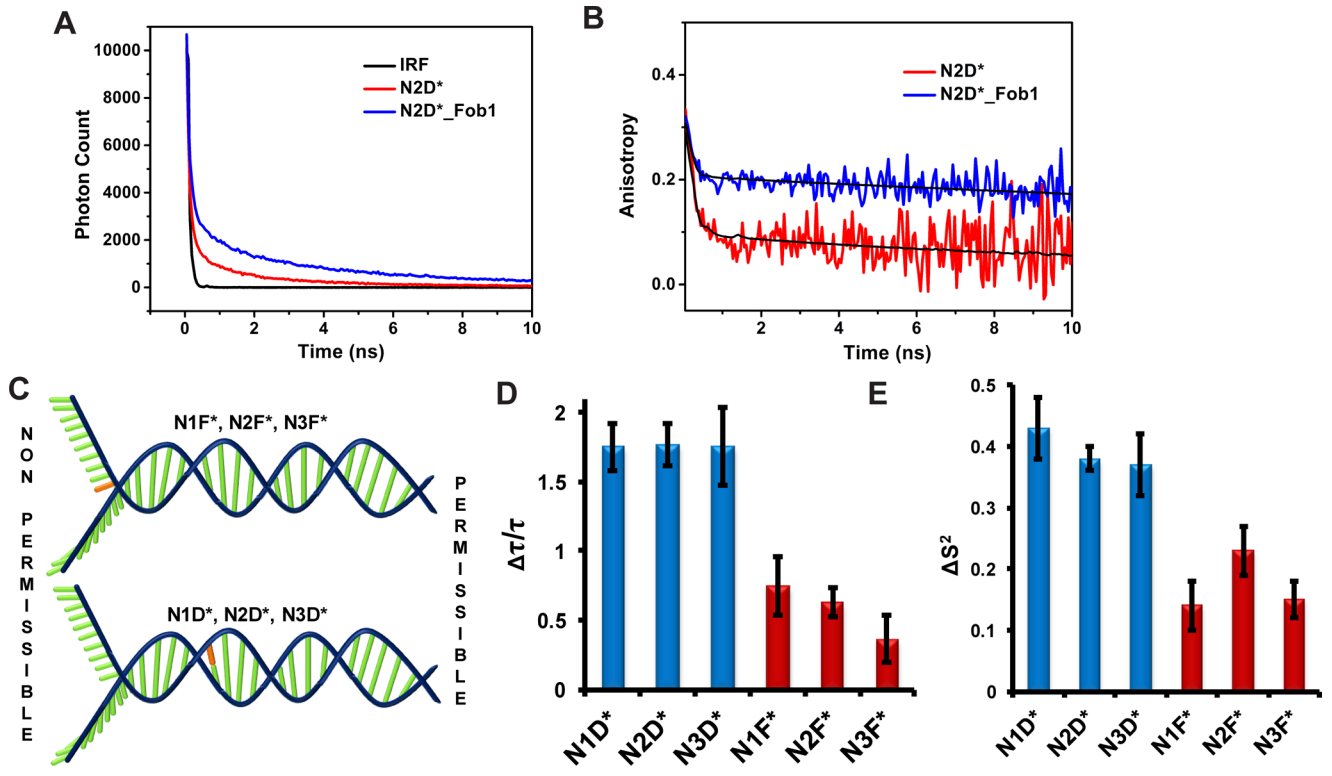

Figure 4. Architectural preferences of Fob1. (A) Binding of Fob1 to the double-stranded RFB1 sequence showing increase in the fluorescence lifetime of 2-AP. (B) Fluorescence anisotropy decay of 2-AP in double-stranded RFB1 with and without Fob1. (C) Cartoon representation of prosthetic forks; 2-AP position is highlighted in orange. (D, E) Fractional increase in the mean lifetime and order parameter, respectively, in the presence of Fob1. The bars in blue represent 2-AP at base-paired positions and in red at the fork junctions.

could be interpreted to indicate the change in the strength of base-pairing.

Our studies reveal a unique observation for 2-AP at the fork positions: an enhancement in the mean fluorescence lifetime when compared to that for the single-stranded DNA was observed for all of the fork positions irrespective of the direction or position of the fork within *ter*1 (Tables 1 and S1). This is in sharp contrast to the decrease in the mean lifetime for 2-AP located at base-pairing locations (Table 1) on going from single-stranded to double-stranded DNA. For example, for sequence N2F*_ss, where the natural adenine is replaced by 2-AP at the 10th position, the enhancement in the mean lifetime from 0.45 to 1.1 ns was observed for the same base in the single-stranded versus forked structure, respectively (Figure 2A,B). This behavior at the forks is reminiscent of an earlier report of a higher fluorescence intensity of 2-AP when presented in a fork.[23,24] Because the 2-AP at the fork junction is in a constricted environment, an enhancement in the lifetime was observed (Tables 1 and S1) for all of the fork positions irrespective of the direction or position of the fork. The cause of this behavior lies in the unique position that the base is presented with: between a rigid double-stranded region and a

DOI: 10.1021/acsomega.7b01117
ACS Omega 2017, 2, 7389−7399

Table 2. Fluorescence Lifetime Parameters for 2-AP Incorporated in Constructs N1D*, N2D*, N3D*, P4D*, P1D*, NtD*, PtD*, Ct1, and Ct2 in Single-Stranded, Double-Stranded, and DNA−Protein Complex

	fluorescence lifetime τ_i in ns (amplitude, α_i)					
sample	τ_1 (α_1)	τ_2 (α_2)	τ_3 (α_3)	τ_4 (α_4)	mean lifetime, τ_m (ns)	$\Delta\tau/\tau$
N1D*_ss	0.047 ± 0.003 (0.76 ± 0.01)	0.55 ± 0.01 (0.13 ± 0.01)	1.93 ± 0.09 (0.074 ± 0.002)	6.50 ± 0.17 (0.039 ± 0.001)	0.50 ± 0.01	
N1D*_ds	0.021 ± 0.003 (0.88 ± 0.01)	0.61 ± 0.09 (0.041 ± 0.003)	2.90 ± 1.05 (0.026 ± 0.004)	9.50 ± 0.77 (0.048 ± 0.002)	0.57 ± 0.02	1.75
N1D*_ds_Fob1	0.044 ± 0.005 (0.57 ± 0.02)	0.57 ± 0.01 (0.15 ± 0.01)	2.36 ± 0.020 (0.14 ± 0.01)	8.06 ± 0.02 (0.14 ± 0.01)	1.57 ± 0.09	
N2D*_ss	0.29 ± 0.05 (0.51 ± 0.01)	1.68 ± 0.17 (0.13 ± 0.01)	7.85 ± 0.06 (0.34 ± 0.03)		3.16 ± 0.14	
N2D*_ds	0.035 ± 0.006 (0.96 ± 0.01)	0.31 ± 0.09 (0.023 ± 0.001)	1.37 ± 0.25 (0.015 ± 0.002)	5.70 ± 0.68 (0.005 ± 0.001)	0.09 ± 0.005	1.78
N2D*_ds_Fob1	0.029 ± 0.002 (0.91 ± 0.01)	0.37 ± 0.03 (0.043 ± 0.003)	1.85 ± 0.18 (0.023 ± 0.001)	6.49 ± 0.23 (0.026 ± 0.001)	0.25 ± 0.01	
N3D*_ss	0.076 ± 0.015 (0.49 ± 0.04)	0.53 ± 0.13 (0.18 ± 0.03)	3.03 ± 0.71 (0.078 ± 0.012)	8.25 ± 0.16 (0.25 ± 0.01)	2.43 ± 0.08	
N3D*_ds	0.013 ± 0.003 (0.93 ± 0.01)	0.20 ± 0.05 (0.030 ± 0.008)	1.51 ± 0.04 (0.013 ± 0.001)	8.94 ± 0.03 (0.024 ± 0.001)	0.25 ± 0.01	1.76
N3D*_ds_Fob1	0.038 ± 0.011 (0.85 ± 0.01)	0.54 ± 0.12 (0.047 ± 0.003)	2.72 ± 0.16 (0.036 ± 0.001)	8.06 ± 0.13 (0.066 ± 0.007)	0.69 ± 0.07	
P4D*_ss	0.076 ± 0.016 (0.61 ± 0.01)	0.43 ± 0.05 (0.19 ± 0.01)	1.96 ± 0.12 (0.14 ± 0.01)	4.91 ± 0.09 (0.061 ± 0.006)	0.70 ± 0.05	
P4D*_ds	0.12 ± 0.01 (0.98 ± 0.01)	1.13 ± 0.06 (0.010 ± 0.001)	6.12 ± 0.19 (0.005 ± 0.001)		0.16 ± 0.01	0.38
P4D*_ds_Fob1	0.14 ± 0.002 (0.98 ± 0.001)	1.28 ± 0.06 (0.014 ± 0.001)	6.10 ± 0.12 (0.011 ± 0.001)		0.22 ± 0.01	
P1D*_ds	0.020 ± 0.006 (0.84 ± 0.01)	0.360 ± 0.07 (0.066 ± 0.005)	2.14 ± 0.03 (0.033 ± 0.005)	8.79 ± 0.25 (0.062 ± 0.004)	0.69 ± 0.08	0.94
P1D*_ds_Fob1	0.035 ± 0.006 (0.67 ± 0.04)	0.71 ± 0.48 (0.11 ± 0.01)	2.24 ± 0.29 (0.092 ± 0.010)	7.94 ± 0.19 (0.13 ± 0.02)	1.34 ± 0.15	
NtD*_ds	0.063 ± 0.016 (0.64 ± 0.04)	1.28 ± 0.08 (0.11 ± 0.01)	8.73 ± 0.06 (0.24 ± 0.03)		2.28 ± 0.30	0.41
NtD*_ds_Fob1	0.10 ± 0.02 (0.48 ± 0.04)	1.73 ± 0.06 (0.18 ± 0.01)	8.40 ± 0.04 (0.34 ± 0.03)		3.21 ± 0.26	
PtD*_ds	0.033 ± 0.004 (0.84 ± 0.01)	0.25 ± 0.02 (0.10 ± 0.01)	1.44 ± 0.04 (0.045 ± 0.004)	5.02 ± 0.20 (0.015 ± 0.001)	0.19 ± 0.01	0.47
PtD*_ds_Fob1	0.031 ± 0.002 (0.84 ± 0.02)	0.20 ± 0.02 (0.085 ± 0.009)	1.69 ± 0.08 (0.043 ± 0.005)	6.46 ± 0.11 (0.025 ± 0.003)	0.28 ± 0.02	
Ct1_ss	0.21 ± 0.13 (0.33 ± 0.09)	0.99 ± 0.34 (0.43 ± 0.03)	3.16 ± 0.77 (0.18 ± 0.04)	7.12 ± 0.24 (0.061 ± 0.009)	1.50 ± 0.12	
Ct1_ds	0.051 ± 0.012 (0.80 ± 0.06)	0.20 ± 0.08 (0.15 ± 0.06)	1.55 ± 0.21 (0.027 ± 0.002)	8.56 ± 0.05 (0.021 ± 0.001)	0.29 ± 0.02	0.62
Ct1_ds_Fob1	0.061 ± 0.008 (0.80 ± 0.02)	0.26 ± 0.05 (0.12 ± 0.03)	1.78 ± 0.08 (0.036 ± 0.002)	7.85 ± 0.03 (0.041 ± 0.002)	0.47 ± 0.02	
Ct2_ds	0.047 ± 0.005 (0.77 ± 0.02)	0.15 ± 0.016 (0.19 ± 0.02)	1.40 ± 0.15 (0.021 ± 0.001)	8.73 ± 0.21 (0.019 ± 0.001)	0.26 ± 0.01	0.7
Ct2_ds_Fob1	0.060 ± 0.013 (0.78 ± 0.04)	0.22 ± 0.05 (0.15 ± 0.04)	1.67 ± 0.17 (0.034 ± 0.001)	7.98 ± 0.13 (0.038 ± 0.001)	0.44 ± 0.03	

DOI: 10.1021/acsomega.7b01117
ACS Omega 2017, 2, 7389−7399

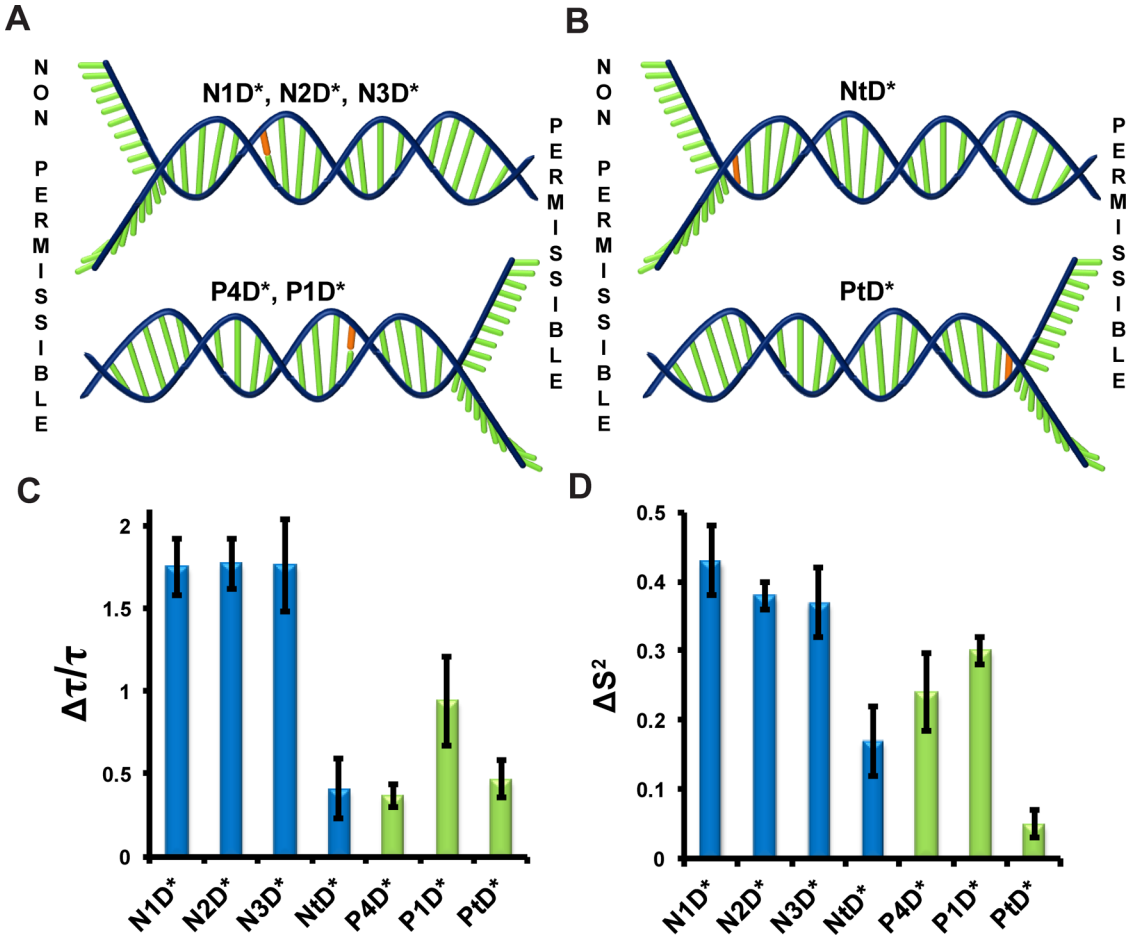

Figure 5. Fob1 perceives the directionality of the forks. (A, B) Cartoon representation of forks, demonstrating the positions of 2-AP in orange. (C, D) Fractional increase in the mean lifetime and the order parameter, respectively, in the presence of Fob1. The bar graphs in blue and green represent 2-AP in base-paired regions of nonpermissible and permissible forks, respectively.

more flexible single-stranded region. The base is unable to stack well with either region, leading to a lower level of quenching. We believe that this unique change in lifetime is a signature property of the fork and can be used in general to detect fork-like structures.

Effect of Fork Direction on *ter*1. Before proceeding to Fob1-mediated polar arrest, we wanted to test whether in the absence of the protein the *ter*1 sequence inherently possesses any property toward polar unwinding. Thermal melting profiles of various prosthetic forks (Figure 3A,B) show that an early melting occurs for the constructs with the fork situated in the permissible direction and a comparatively higher melting temperature is observed for the oppositely directed forks, clearly indicating that in these short constructs the partially unthreaded permissible forks are easier to open than the nonpermissible ones. A closer look at the sequence reveals that this differential melting occurs because of the skewed distribution of the G−C base pairs. Analyzing other RFBs reveal that Fob1-binding sequences consistently contain this skewed distribution (Figure S4). This is particularly striking because this mode is very different from other fork-blocking systems like the *ter* sequences in *E. coli* and *Bacillus subtilis*. In contrast to eukaryotes, the *ter* sequences in prokaryotic systems show high degree of homology and have conserved bases that serve as signature sequences.[5,25]

Fob1 Binding Causes Larger Perturbation to the Double-Stranded Region. After analyzing the motional dynamics of various 2-AP prosthetic forks in detail, the Fob1 protein was added to these sequences. Information regarding differential perturbation of bases (double-stranded vs forked region) caused by Fob1 binding was the first question that was addressed. All experiments were performed under saturating conditions (28 μM Fob1, see Figure 1B). This was to ensure that the Fob1−DNA complexed state is the predominant form. The sequences were designed such that 2-AP was incorporated within the double-stranded region at positions 5, 7, and 4 from the fork (N1D*, N2D*, and N3D*, respectively; Figure 4C) or at the fork positions itself (N1F*, N2F*, and N3F*; Figure 4C). It was observed that the fractional increase in the mean lifetime of 2-AP on Fob1 binding (Figure 4A,D) in all of the cases exhibited a larger change for the probe present within the double-stranded regions of the prosthetic forks. The sensitivity of this region was also reflected from the comparatively larger increase in dynamic restriction in the local motion (Figure 4B), which was on an average 1.5−2-fold higher than that for the bases present at the fork regions (Table 1, Figure 4E). Restriction in the motional freedom of 2-AP due to protein binding is also evident from the decrease in the amplitude associated with the faster correlation time (Figure 4E, Table S2).

DOI: 10.1021/acsomega.7b01117
ACS Omega 2017, 2, 7389−7399

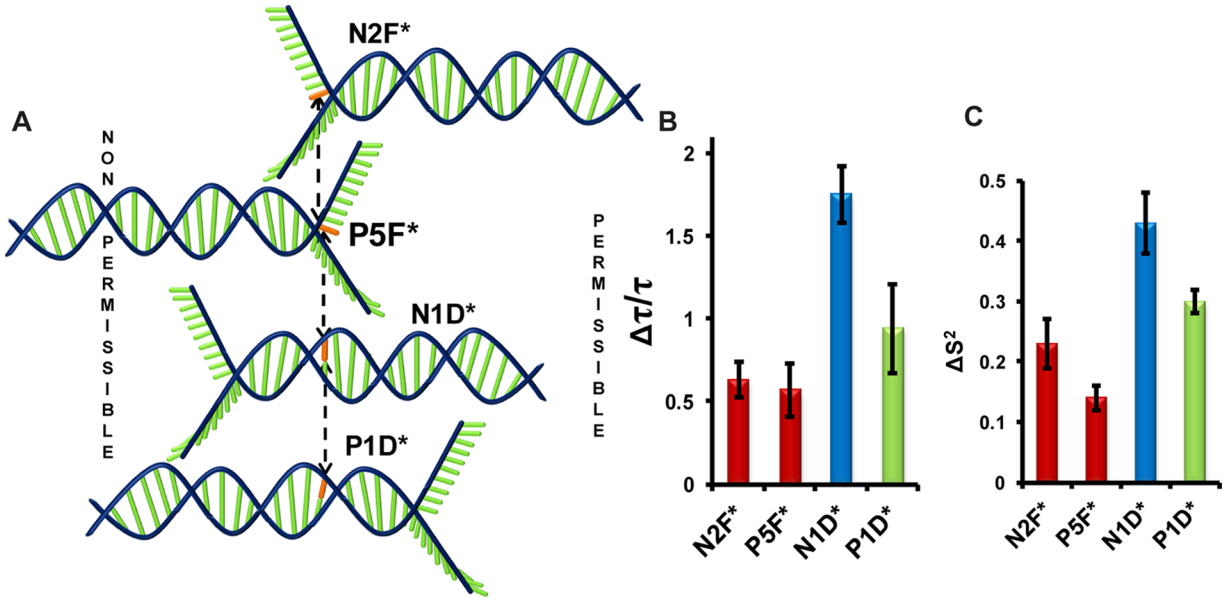

Figure 6. Preferential binding of Fob1 to the nonpermissible end is not influenced by local 2-AP position. (A) Cartoon representation of forks demonstrating the positions of 2-AP in orange. (B, C) Fractional increase in the mean lifetime and order parameter, respectively, in the presence of Fob1. The bars in red represent 2-AP located in oppositely directed forks at fork junctions and in blue and green at the base-paired position.

It should be pointed out that the change in motional dynamics (ΔS^2) is a more robust indicator of the extent of perturbation caused by Fob1 binding when compared with the fractional increase in the mean lifetime because the mean lifetime is sensitive to DNA architecture. Furthermore, if the extents of perturbation of the double-stranded and fork regions are very similar, we should have seen a larger value of ΔS^2 for the fork sites when compared to that for the double-stranded region, contrary to the observations (Figure 4E). This is because the bases at the fork positions are relatively less stacked and therefore Fob1 binding at this position should have resulted in greater restriction. However, because the results indicate that Fob1 binding consistently perturbs the double-stranded region more significantly as compared with the fork positions, we can conclude that Fob1 binds preferentially to this architecture. Moreover, it was noted that the increase in the mean fluorescence lifetime of 2-AP on going from ds-DNA to ds-DNA−Fob1 complex arises mainly from a decrease in the amplitude of the shortest lifetime and a concomitant increase in the amplitude of the longest lifetime (Table 2). As mentioned earlier, the decrease in the amplitude of the shortest lifetime is an indication of Fob1-binding-caused weakening of the stacking interaction of 2-AP with the neighboring base (Table 1). The longest lifetime component of ds-DNA does not change significantly on binding to the protein. However, the amplitude of the longest component increases on protein binding; this is due to the perturbation caused by protein binding, resulting in an increase in the population of the extrahelical component, a consequence of partial opening of the helix. From the above observations, it is clear that Fob1 latches ahead of the fork position within the double-stranded region of the construct.

Polarity of Fob1 Binding to DNA. The experiments performed above clearly demonstrated that Fob1 binding perturbs the double-stranded DNA architecture over fork junction positions. The next question asked is whether Fob1 shows any preference for forks arriving from the opposite directions. This question is the central theme of this work. Two sets of constructs were designed (Figure 5A,B) such that 2-AP's were positioned in the base-paired region with the fork approaching from the nonpermissible (N1D*, N2D*, N3D*, and NtD*) or the permissible end (P4D*, P1D*, and PtD*). A comparison of the fractional change in the mean lifetime (Figure 5C) showed that the base-paired positions in constructs with forks progressing from the nonpermissible direction face a greater perturbation as compared to that for those from the permissible direction. In some cases, the difference in lifetime between the permissible versus nonpermissible-directed forks is greater than 4-fold. A greater change in the order parameter was also observed for 2-AP in the nonpermissible forks compared to that in the permissible forks (Figure 5D). This difference is likely caused by the larger extent of perturbation to base stacking, as well as the reduction in the space available for local motion of the base, for the forks in the nonpermissible direction. The enhanced changes for the nonpermissible-directed forks indicate a stronger interaction of the DNA−protein complex for these constructs, thereby resulting in slower dissociation of the complex. It is worth noting that for creating a polar block the difference in the rate of dissociation of the Fob1−DNA complex rather than the difference in binding affinity is more relevant. This has been observed earlier where surface plasmon resonance studies on the polarity of termination of replication in the *E. coli* Tus-*Ter* system revealed the importance of the dissociation rate in explaining the mechanism of polarity difference.[5] Therefore, the above observations assert that Fob1 perceives the directionality of the forks and that there exists an asymmetric mode of binding of Fob1 to DNA. The protein possibly differentiates between the permissible and nonpermissible directions of *ter*1 and binds such that the two ends of *ter*1 interact and perceive a different face of the protein. Because of its differential mode of binding of oppositely directed forks, the protein would provide an easier route for the passage of a fork progressing from the permissive direction, whereas impede the progress on the nonpermissive side, leading to polar stalling of replication forks.

To confirm that the preferential perturbation effects of Fob1 are not due to local 2-AP position but solely due to

DOI: 10.1021/acsomega.7b01117
ACS Omega 2017, 2, 7389−7399

directionality, fork constructs where the position of 2-AP in the double-stranded or fork sequence remains constant but the direction of the forks is different were made (Figure 6A, Table 1). Interaction of Fob1 with these different DNA architectures, in terms of both the fluorescence dynamic parameters, reveals that Fob1-binding-caused perturbation follows the order N1D* > P1D* > N2F* > P5F* (Figure 6B,C). Thus, the protein distinguishes between the constructs and, as established before, Fob1 favors the double-stranded region of a construct with forks directed from the nonpermissible end over the permissible directed forks. Overall, it can be inferred from here that the nature of protein binding is related to not only the sequence but also the DNA architecture that is being presented to it.

Fob1 Polarity Is Sequence-Specific. Finally, to ascertain the specificity of the results seen with the prosthetic forks in *ter*1, two random constructs created with forks on opposite sides were studied as control sequences (Figure S5A, Ct1_ds and Ct2_ds). The control sequence was designed such that the position of 2-AP remains constant and after annealing with partially complementary sequences, the pair of oppositely directed forks generated possess equal number of G−C base pairs in the double-stranded region. The fluorescence dynamic parameters (Tables 2 and S2) show very similar binding properties, with the differences being indistinguishable (Figure S5B,C). The results reveal the absence of any preferential extent of perturbation by Fob1 to the two control sequences. The observations clearly indicate that the binding prejudices that we observe for the oppositely directed forked constructs of *ter*1 are caused by specific interactions of Fob1 with this sequence.

Insights into the Mechanism of Polar Arrest by Fob1. In this work, the aim was to investigate if Fob1 can sense a polar block in a standalone setting or does it require a host of other proteins to exert this effect. By employing 2-AP, a highly environmentally sensitive site-specific fluorescence probe, into a series of artificial DNA forked structures, it was established that Fob1 can indeed create a unidirectional block. This strategy of incorporation of 2-AP into replication forks has been successfully employed earlier to identify the DNA breathing events at the fork junctions as well as the GTP-dependent helicase activity-dependent interaction of primosome at the replication fork.[23,24] Corroborating thermal melting studies showed that the choice of RFB as a blocking sequence is not arbitrary, rather a specific arrangement of bases termed as "sequence effect", which is possibly one of the contributors to the fork polarity. This effect is magnified by the presence of Fob1, which possesses the ability of sensing differentially directed forks. Fob1 acts like a clamp, few base pairs ahead of the fork, and via preferential interaction with the double-stranded region at the nonpermissible end acts like a polar barrier. Reasoning from the converse behavior it manifests on the DNA unthreading from opposite directions, it is likely that Fob1 binds DNA in an asymmetric manner, posing different faces on either end of the sequence. During replication, the progress of a fork toward a particular base tends to cause a decrease in the stacking interactions that is sensed by Fob1. On perceiving the direction of approaching fork, Fob1 accordingly alters its mode of binding, enhancing its hold on the sequence for a fork approaching from the nonpermissible direction, whereas allowing progression of the fork from the permissible side and thus bringing about polarity. The larger restriction in the nonpermissible direction would necessitate a larger force to remove the protein, resulting in slower dissociation of the complex in this orientation for fork progress. As mentioned above, in this scenario, the difference in the rate of dissociation of the Fob1−DNA complex rather than the difference in the binding affinity is the dominant controlling factor for polarity-based mechanisms in DNA−protein interactions, as noted in earlier studies.[5] In an in vivo setting, we believe that Fob1 possibly strengthens this barrier in consort with other proteins. The event can be multistep where Fob1 first forms a terminator complex at the RFB site and then recruits the other members. The biophysical analysis of the Fob1-RFB system, along with the use of 2-AP, provides a precise site-specific resolution in studies pertaining to these events. We believe that the site-specific fluorescence dynamics is an invaluable tool used here to obtain insights into the binding footprints of proteins on their cognate sequences, in greater detail.

MATERIALS AND METHODS

Cloning and Protein Purifications. Due to problems of low expression of the Fob1 protein from *S. cerevisiae*, studies with the homologous Fob1 system of *Ashbya gossypii* were initiated. For the experiments, Fob1 (1−450 residues) that comprises the DNA binding region was cloned in a modified pET vector, with an N-terminal hexahistidine tag. Plasmids were transformed in Rosetta cells and grown in Luria Bertani broth with antibiotics chloramphenicol and kanamycin at concentrations 30 and 35 μg/mL, respectively, at 37 °C and 250 rpm. Protein expression was induced with IPTG (isopropyl β-D-1-thiogalactopyranoside) at 0.8 mM concentration. The induced cells were grown for about 6 h at 25 °C and harvested. The cells were resuspended in buffer A (50 mM HEPES, pH 7.5, 500 mM NaCl, 5 mM imidazole) and homogenized by sonication. After removal of cell debris by centrifugation at 20 000 rpm and 4 °C, the supernatant was added to Ni-NTA beads (GE Healthcare, WI) that had been equilibrated in buffer A. The beads were subsequently separated by centrifugation and mounted on a column, followed by a slow wash with wash buffer (50 mM HEPES, pH 7.5, 500 mM NaCl, 15 mM imidazole). The protein was eluted with the buffer containing imidazole at 200 mM (50 mM HEPES, pH 7.5, 300 mM NaCl, 200 mM imidazole). The eluted protein was desalted using desalting columns (Econo-Pac10DG columns, Bio-Rad) into a buffer containing 35 mM HEPES, pH 7.5, 250 mM NaCl, 3% glycerol, and 1 mM DTT and used for the fluorescence studies.

DNA Synthesis and Annealing. Modified (Table 1 and Figures S2 and S3) and unmodified DNA sequences were purchased from Integrated DNA Technologies. The oligonucleotides were quantified by employing a spectrophotometer (GE, GeneQuant 1300, WI) at 260 nm. The complementary strands of the modified (2-AP incorporated) DNA were taken in 20% excess, so as to ensure complete annealing of the latter. For the unmodified constructs, the complementary strands were taken in an equimolar ratio. The DNA sequences were annealed in the presence of 1× annealing buffer (5 mM Tris, pH 7.5, 15 mM NaCl). The mixture was subjected to a temperature of 95 °C for 5 min by placing in a water bath, which was then allowed to cool slowly to room temperature. The samples were stored at −20 °C.

Electrophoretic Mobility Shift Assay (EMSA). The oligonucleotides were labeled with radioactive ^{32}P as the phosphate group at the 5′ end of the DNA. Approximately, 1 nmol of the labeled oligonucleotide was incubated with the protein (purified in 35 mM HEPES, pH 7.5, 200 mM NaCl, 3%

DOI: 10.1021/acsomega.7b01117
ACS Omega 2017, 2, 7389−7399

glycerol) concentrations ranging from 4.2 μM to 65 nM obtained by 2-fold serial dilution in a total of 10 μL of reaction mixture. The incubation mixture also contained 10 mM Tris–HCl (pH 7.8), 50 mM KCl, 1.8 mM DTT, 2 μg/mL hemoglobin, and 7.4% glycerol. After 30 min of incubation at 25 °C, the samples were run in a 6% nondenaturing polyacrylamide gel with TBE as the running buffer (89 mM Tris-base, pH 8.3, 89 mM boric acid, 2 mM EDTA) at 100 V and 4 °C. Gels were analyzed by phosphorimaging using Storm 625 (GE healthcare) and software ImageQuant (GE).

Thermal Melting of DNA. DNA thermal melting studies were carried out in a Varian Cary 100 Bio UV–visible spectrophotometer. DNA was taken at ~2 μM concentration in a buffer containing 20 mM phosphate buffer, pH 7.4, 100 mM NaCl, and 1 mM EDTA. The absorbance of the samples was monitored at 260 nm wavelength as the temperature was raised from 20 to 95 °C at the rate of 1 °C/min.

Time-Resolved Fluorescence. The time-resolved fluorescence decay and anisotropy decay measurements were performed with a Rhodamine 6G dye laser that generates pulses of 1 ps width.[18,22,26,27] The dye laser was driven by a passively mode-locked frequency-doubled Nd:YAG laser (Vanguard, Spectra Physics). The samples were excited with the second-harmonic output of the angle-tuned KDP crystal (310 nm). The curves for fluorescence decay were obtained from a time-correlated single-photon counting setup coupled to a microchannel plate photomultiplier (model 2809U, Hamamatsu Corp.). The instrument response function (IRF) was obtained at 310 nm from a very dilute colloidal suspension of dried nondairy coffee whitener. The IRF half-width was ~40 ps. The fluorescence emission of the samples was collected through a 345 nm cut-off filter followed by a monochromator at 370 nm with a collection bandwidth of 3 nm. The number of counts in the peak channel was ~10 000. The fluorescence emission for obtaining the lifetime was monitored at 54.7° (magic angle) to avoid contribution from anisotropy decay. The emission in directions parallel and perpendicular to that of the incident polarized light was collected for the time-resolved anisotropy measurements.

The samples consisted of 7 μM oligonucleotides, with and without the protein at 28 μM concentration. The complex was incubated at room temperature for 15 min before data collection. The buffer consisted of 35 mM HEPES, pH 7.5, 250 mM NaCl, 3% glycerol, and 1 mM DTT.

Data Analysis. *Analysis of Fluorescence Decay Kinetics.* Analysis of the fluorescence decay for the lifetime measurements was performed using a nonlinear least-squares iterative deconvolution method based on the Levenberg–Marquardt algorithm and expressed as a sum of exponentials with the following equation

$$I(t) = \sum \alpha_i \exp(-t/\tau_i) \tag{1}$$

where α_i is the amplitude of the ith component associated with fluorescence lifetime τ_i such that $\sum \alpha_i = 1$. The mean lifetime, τ_m, of the system is obtained from $\sum \alpha_i \tau_i$.

Analysis of Fluorescence Anisotropy Decay Kinetics. The time-resolved anisotropy decay curves were derived from experimentally obtained $I_{\parallel}(t)$ and $I_{\perp}(t)$ with the following equation

$$r(t) = \frac{I_{\parallel}(t) - G(\lambda) I_{\perp}(t)}{I_{\parallel}(t) + 2G(\lambda) I_{\perp}(t)} \tag{2}$$

where $r(t)$ is the time-dependent anisotropy, $G(\lambda)$ is the geometry factor at the wavelength of emission, λ, and $I_{\parallel}(t)$ and $I_{\perp}(t)$ are the fluorescence intensities collected with the emission polarizer at 0° (parallel) and 90° (perpendicular) with respect to excitation, respectively. The value of $G(\lambda)$ for the optics for measuring emission was calculated independently using 50 μM solution of 2-AP.

The fluorescence anisotropy decay analysis was performed by globally fitting $I_{\parallel}(t)$ and $I_{\perp}(t)$ as

$$I_{\parallel}(t) = I(t)[1 + 2r(t)]/3 \tag{3}$$

$$I_{\perp}(t) = I(t)[1 - r(t)]/3 \tag{4}$$

$$r(t) = r_0[\beta_1 \exp(-t/\phi_1) + \beta_2 \exp(-t/\phi_2)] \tag{5}$$

where r_0 is the anisotropy in the absence of any rotational diffusion and β_i is the amplitude associated with the ith rotational correlation times ϕ_i, such that $\sum \beta_i = 1$. ϕ_1 represents the local motion of the fluorophore, and ϕ_2 represents the global motion of DNA or the DNA–Fob1 complex. The model assumes that the sample contains a population having uniform motional dynamics properties with each species associated with two rotational correlation times. The r_0 value was estimated to be 0.31 in a separate experiment with a sample in 70% glycerol. For the analysis of anisotropy decays, the r_0 value of 0.31 with a window of 0.01 was used. Anisotropy parameters ϕ_i and β_i were estimated by analyzing, globally, $I_{\parallel}(t)$ and $I_{\perp}(t)$ using eqs 3 and 4 by fixing r_0 (as mentioned above) and intensity decay parameters estimated by analyzing the decay obtained at the magic angle by eq 1. This procedure enabled us to reduce the number of free parameters in eqs 3 and 4 and thereby enhanced the robustness of the recovery of anisotropy decay parameters. Errors in the recovered parameters were estimated from a combination of several decay profiles from a sample and multiple samples. All of the decay curves were analyzed independently to obtain stable fits with χ^2 values close to unity and random distribution of residuals.

The extent of restriction of 2-AP motion was estimated from generalized order parameter S^2 given by the following equation[21,28,29]

$$S^2 = \beta_2/(\beta_1 + \beta_2) \tag{6}$$

To compare the changes in the mean lifetime of 2-AP in the constructs, caused by Fob1 binding, the fractional increase in the mean lifetime was assessed by the following formula

$$\Delta\tau/\tau = (\tau_{m,\text{complex}} - \tau_{m,\text{free DNA}})/\tau_{m,\text{free DNA}} \tag{7}$$

The Fob1-binding-induced changes in the spatial restriction to the local motion of 2-AP in DNA constructs were analyzed by

$$\Delta S^2 = (S^2_{\text{complex}} - S^2_{\text{free DNA}}) \tag{8}$$

■ ASSOCIATED CONTENT

Supporting Information

The Supporting Information is available free of charge on the ACS Publications website at DOI: 10.1021/acsomega.7b01117.

Experimental method of steady-state anisotropy, schematic representation of rDNA, sequence design of constructs used in the study, fluorescence lifetime, and anisotropy decay parameters of DNA and DNA–protein complexes containing 2-AP (PDF)

DOI: 10.1021/acsomega.7b01117
ACS Omega 2017, 2, 7389–7399

AUTHOR INFORMATION

Corresponding Authors

*E-mail: gk@tifr.res.in. Tel: 91-7738041952 (G.K.).
*E-mail: ruchi@chem.iitb.ac.in. Tel: 91-22-2576-7165. Fax: 91-22-2576-7152 (R.A.).

ORCID

Ruchi Anand: 0000-0002-2045-3758

Present Address

[‖]Department of Biotechnology, Anna University, Chennai, Tamil Nadu 600025, India (G.K.).

Author Contributions

[§]A.B. and J.M. contributed equally.

Author Contributions

R.A. initiated the idea of the project. R.A. and G.K. designed experiments and wrote the manuscript. A.B. and J.M. performed the experiments, collected data, performed data analysis, and partook in manuscript writing; M.K. assisted in data collection and data analysis; and S.N. assisted in data collection.

Notes

The authors declare no competing financial interest.

ACKNOWLEDGMENTS

The authors thank N. Periasamy for providing the software used in the analysis of time-resolved fluorescence data. G. Krishnamoorthy is a recipient of J.C. Bose National Research Fellowship from the Government of India. The authors also thank IIT Bombay (Mumbai) and TIFR (Mumbai) for providing all of the necessary facilities. This work was supported by Tata Institute of Fundamental Research (Mumbai), Indian Institute of Technology Bombay (Mumbai), Department of Biotechnology, Government of India (BT/PRI3766/BRB/10/785/2010), Board of Research in Nuclear Sciences (No. 37(1)/14/05/2017-BRNS/37039), Council of Scientific and Industrial Research, Government of India (for the fellowship of A.B.), and Department of Biotechnology, Government of India (for DBT-Research Associateship program of J.M.).

REFERENCES

(1) Labib, K.; Hodgson, B. Replication fork barriers: pausing for a break or stalling for time? *EMBO Rep.* **2007**, *8*, 346−353.
(2) Takeuchi, Y.; Horiuchi, T.; Kobayashi, T. Transcription-dependent recombination and the role of fork collision in yeast rDNA. *Genes Dev.* **2003**, *17*, 1497−1506.
(3) Tsang, E.; Carr, A. M. Replication fork arrest, recombination and the maintenance of ribosomal DNA stability. *DNA Repair* **2008**, *7*, 1613−1623.
(4) Kamada, K.; Horiuchi, T.; Ohsumi, K.; Shimamoto, N.; Morikawa, K. Structure of a replication-terminator protein complexed with DNA. *Nature* **1996**, *383*, 598−603.
(5) Mulcair, M. D.; Schaeffer, P. M.; Oakley, A. J.; Cross, H. F.; Neylon, C.; Hill, T. M.; Dixon, N. E. A molecular mousetrap determines polarity of termination of DNA replication in *E. coli*. *Cell* **2006**, *125*, 1309−1319.
(6) Brewer, B. J.; Fangman, W. L. A replication fork barrier at the 3′ end of yeast ribosomal RNA genes. *Cell* **1988**, *55*, 637−643.
(7) Linskens, M. H.; Huberman, J. A. Organization of replication of ribosomal DNA in *Saccharomyces cerevisiae*. *Mol. Cell. Biol.* **1988**, *8*, 4927−4935.
(8) Petes, T. D. Yeast ribosomal DNA genes are located on chromosome XII. *Proc. Natl. Acad. Sci. U.S.A.* **1979**, *76*, 410−414.
(9) Skryabin, K. G.; Eldarov, M. A.; Larionov, V. L.; Bayev, A. A.; Klootwijk, J.; de Regt, V. C. H. F.; Veldman, G. M.; Planta, R. J.; Georgiev, O. I.; Hadjiolov, A. A. Structure and function of the nontranscribed spacer regions of yeast rDNA. *Nucleic Acids Res.* **1984**, *12*, 2955−2968.
(10) Johzuka, K.; Horiuchi, T. Replication fork block protein, Fob1, acts as an rDNA region specific recombinator in *S. cerevisiae*. *Genes Cells* **2002**, *7*, 99−113.
(11) Sinclair, D. A.; Guarente, L. Extrachromosomal rDNA circles–a cause of aging in yeast. *Cell* **1997**, *91*, 1033−1042.
(12) Dlakić, M. A model of the replication fork blocking protein Fob1p based on the catalytic core domain of retroviral integrases. *Protein Sci.* **2002**, *11*, 1274−1277.
(13) Kobayashi, T. The replication fork barrier site forms a unique structure with Fob1p and inhibits the replication fork. *Mol. Cell. Biol.* **2003**, *23*, 9178−9188.
(14) Brewer, B. J.; Lockshon, D.; Fangman, W. L. The arrest of replication forks in the rDNA of yeast occurs independently of transcription. *Cell* **1992**, *71*, 267−276.
(15) Kobayashi, T.; Hidaka, M.; Nishizawa, M.; Horiuchi, T. Identification of a site required for DNA replication fork blocking activity in the rRNA gene cluster in *Saccharomyces cerevisiae*. *Mol. Gen. Genet.* **1992**, *233*, 355−62.
(16) Holz, B.; Klimasauskas, S.; Serva, S.; Weinhold, E. 2-Aminopurine as a fluorescent probe for DNA base flipping by methyltransferases. *Nucleic Acids Res.* **1998**, *26*, 1076−1083.
(17) Rachofsky, E. L.; Osman, R.; Ross, J. B. A. Probing structure and dynamics of DNA with 2-aminopurine: effects of local environment on fluorescence. *Biochemistry* **2001**, *40*, 946−956.
(18) Ramreddy, T.; Kombrabail, M.; Krishnamoorthy, G.; Rao, B. J. Site-specific dynamics in TAT triplex DNA as revealed by time-domain fluorescence of 2-aminopurine. *J. Phys. Chem. B* **2009**, *113*, 6840−6846.
(19) Ramreddy, T.; Rao, B. J.; Krishnamoorthy, G. Site-specific dynamics of strands in ss- and dsDNA as revealed by time-domain fluorescence of 2-aminopurine. *J. Phys. Chem. B* **2007**, *111*, 5757−5766.
(20) Subuddhi, U.; Hogg, M.; Reha-Krantz, L. J. Use of 2-aminopurine fluorescence to study the role of the beta hairpin in the proofreading pathway catalyzed by the phage T4 and RB69 DNA polymerases. *Biochemistry* **2008**, *47*, 6130−6137.
(21) Lipari, G.; Szabo, A. Effect of librational motion on fluorescence depolarization and nuclear magnetic resonance relaxation in macromolecules and membranes. *Biophys. J.* **1980**, *30*, 489−506.
(22) Nag, N.; Rao, B. J.; Krishnamoorthy, G. Altered dynamics of DNA bases adjacent to a mismatch: a cue for mismatch recognition by MutS. *J. Mol. Biol.* **2007**, *374*, 39−53.
(23) Jose, D.; Datta, K.; Johnson, N. P.; von Hippel, P. H. Spectroscopic studies of position-specific DNA "breathing" fluctuations at replication forks and primer-template junctions. *Proc. Natl. Acad. Sci. U.S.A.* **2009**, *106*, 4231−4236.
(24) Jose, D.; Weitzel, S. E.; von Hippel, P. H. Breathing fluctuations in position-specific DNA base pairs are involved in regulating helicase movement into the replication fork. *Proc. Natl. Acad. Sci. U.S.A.* **2012**, *109*, 14428−14433.
(25) Griffiths, A. A.; Andersen, P. A.; Wake, R. G. Replication terminator protein-based replication fork-arrest systems in various *Bacillus* species. *J. Bacteriol.* **1998**, *180*, 3360−3367.
(26) Goel, T.; Mukherjee, T.; Rao, B. J.; Krishnamoorthy, G. Fluorescence dynamics of double- and single-stranded DNA bound to histone and micellar surfaces. *J. Phys. Chem. B* **2010**, *114*, 8986−8993.
(27) Singh, T. S.; Rao, B. J.; Krishnamoorthy, G. GTP binding leads to narrowing of the conformer population while preserving the structure of the RNA aptamer: a site-specific time-resolved fluorescence dynamics study. *Biochemistry* **2012**, *51*, 9260−9269.
(28) Avilov, S. V.; Piemont, E.; Shvadchak, V.; de Rocquigny, H.; Mely, Y. Probing dynamics of HIV-1 nucleocapsid protein/target hexanucleotide complexes by 2-aminopurine. *Nucleic Acids Res.* **2008**, *36*, 885−896.

DOI: 10.1021/acsomega.7b01117
ACS Omega 2017, 2, 7389−7399

(29) Rai, P.; Cole, T. D.; Thompson, E.; Millar, D. P.; Linn, S. Steady-state and time-resolved fluorescence studies indicate an unusual conformation of 2-aminopurine within ATAT and TATA duplex DNA sequences. *Nucleic Acids Res.* **2003**, *31*, 2323−2332.

DOI: 10.1021/acsomega.7b01117
ACS Omega 2017, 2, 7389−7399